Performance of astronomical beam combiner prototypes fabricated by hybrid sol-gel technology

Askari Ghasempour[1,2,3,4,*], A.M.P. Leite[1], D. Alexandre[1,2,5], F. Reynaud[4], P.V.S. Marques[1,2], P.J.V. Garcia[3,6], and P.J.Moreira[2]

[1]*Dep. de Física e Astronomia, Faculdade de Ciências, Universidade do Porto, Portugal*
[2]*Unidade de Optoelectrónica e Sistemas Electrónicos - INESC Porto, Portugal*
[3]*Faculdade de Engenharia, Laboratório de Sistemas, Instrumentação e Modelação em Ciências e Tecnologias do Ambiente e do Espaço, Universidade do Porto, Portugal*
[4]*XLIM Département Photonique, UMR CNRS 6172, France*
[5]*Dep.de Física, Universidade de Trás-os-Montes e Alto Douro, Portugal*
[6]*Université Joseph Fourier - Grenoble 1 / CNRS, Laboratoire d'Astrophysique de Grenoble, UMR 5571, BP 53, 38041 Grenoble Cedex 09, France*
[*]*askari@fc.up.pt*

Abstract: Integrated optics coaxial two, three and four telescope beam combiners have been fabricated by hybrid sol-gel technology for astronomical applications. Temporal and spectral analyses of the output interferometric signal have been performed, and their results are in mutual good agreement. The results of the characterization method employed are cross-checked using contrast measurements obtained independently, demonstrating that the chromatic differential dispersion is the main contributer to contrast reduction. The mean visibility of the fabricated devices is always higher than 95 %, obtained using a source with spectral bandwidth of 50 nm. These results show the capability of hybrid sol-gel technology for fast prototyping of complex chip designs used in astronomical applications.

OCIS codes: (120.3180) Interferometry; (130.3120) Integrated optics devices; (130.5460) Polymer waveguides; (160.6060) Solgel; (350.1260) Astronomical optics.

References and links

1. J. D. Monnier, "Optical interferometry in astronomy," Rep. Prog. Phys. **66**, 789-857 (2003).
2. J. Bland-Hawthorn, M. Englund, and G. Edvell, "New approach to atmospheric OH suppression using an aperiodic fibre Bragg grating," Opt. Express **12**, 5902-5909 (2004).
3. S. Vergnole, L. Delage, F. Reynaud, L. Labonte, P. Roy, G. Melin, and L. Gasca, "Test of photonic crystal fiber in broadband interferometry," Appl. Opt. **44**, 2496-2500 (2005).
4. R. R. Thomson, A. K. Kar, and J. Allington-Smith, "Ultrafast laser inscription: an enabling technology for astrophotonics," Opt. Express **17**, 1963-1969 (2009).
5. E. Le Coarer, S. Blaize, P. Benech, I. Stefanon, A. Morand, G. Lerondel, G. Leblond, P. Kern, J. M. Fedeli and P. Royer , "Wavelength-scale stationary-wave integrated fourier-transform spectrometry," Nature Photon. **1**, 473-478 (2007).
6. P. Kern, E. Le Coarer, and P. Benech, "On-chip spectrodetection for fully integrated coherent beam combiners," Opt. Express **17**, 1976-1987 (2009).
7. F. Malbet, P. Kern, I. Schanen-Duport, J. P. Berger, K. Rousselet-Perraut and P. Benech, "Integrated optics for astronomical interferometry I. concept and astronomical applications," Astron. Astrophys. Suppl. **138**, 135-145 (1999).
8. J. P. Berger, K. Rousselet-Perraut, P. Kern, F. Malbet, I. Schanen-Duport, F. Reynaud, P. Haguenauer and P. Benech, "Integrated optics for astronomical interferometry - II. first laboratory white-light interferograms," Astron. Astrophys. Suppl. **139**, 173- 177 (1999).

#122663 - $15.00 USD Received 12 Jan 2010; revised 28 Mar 2010; accepted 29 Mar 2010; published 21 Apr 2010

9. P. Haguenauer, J. P. Berger, K. Rousselet-Perraut, P. Kern, F. Malbet, I. Schanen-Duport and P. Benech, "Integrated optics for astronomical interferometry. III. optical validation of a planar optics two-telescope beam combiner," Appl. Opt. **39**, 2130-2139 (2000).
10. K. Rousselet-Perraut, P. Haguenauer, P. Petmezakis, J. P. Berger, D. Mourard, S. Ragland, G. Huss, F. Reynaud, E. Le Coarer, P. Kern and F. Malbet, "Qualification of ionic (integrated optics near-infrared interferometric camera)," in *Interferometry in Optical Astronomy*, P. Léna and A. Quirrenbach, eds., Proc. SPIE **4006**, 1042–1051 (2000).
11. J. P. Berger, P. Haguenauer, P. Kern, K. Perraut, F. Malbet, I. Schanen, M. Severi, R. Millan-Gabet and W. Traub, "Integrated optics for astronomical interferometry - IV. first measurements of stars," Astron. Astrophys. **376**, L31-L34 (2001).
12. J. B. LeBouquin, P. Labeye, F. Malbet, L. Jocou, F. Zabihian, K. Rousselet-Perraut, J. P. Berger, A. Delboulbe, P. Kern, A. Glindemann and M. Schoeller, "Integrated optics for astronomical interferometry VI. coupling the light of the vlti in k band," Astron. Astrophys. **450**, 1259-1264 (2006).
13. M. Benisty, J. P. Berger, L. Jocou, P. Labeye, F. Malbet, K. Perraut and P. Kern, "An integrated optics beam combiner for the second generation VLTI instruments," Astron. Astrophys. **498**, 601-613 (2009).
14. J. B. LeBouquin, J. P. Berger, P. Labeye, E. Tatulli, F. Malber, K. A. Perraut and P. Kern, "Comparison of integrated optics concepts for a near infrared multi-telescope beam combiner," in *New Frontiers in Stellar Interferometry*, A. Traub, ed., Proc. SPIE **5491**, 1362-1369 (2004).
15. L. Jocou, J. P. Berger, F. Malbet, P. Kern, and U. Beckmann, "System overview of the VLTI Spectro-Imager," in *Optical and Infrared Interferometry*, M. Scholler, W. Danchi, and F. Delplancke, eds., Proc. SPIE **7013**, 70132Y-70132Y-12 (2008).
16. J. E. Baldwin, M. G. Beckett, R. C. Boysen, D. Burns, D. F. Buscher, G. C. Cox, C. A. Haniff, C. D. Mackay, N. S. Nightingale, J. Rogers, P. A. G. Scheuer, T. R. Scott, P. G. Tuthill, P. J. Warner, D. M. A. Wilson and R. W. Wilson, "The first images from an optical aperture synthesis array: mapping of Capella with COAST at two epochs," Astron. Astrophys. **306**, L13 (1996).
17. F. Baron, E. Block, D. F. Buscher, J. Coyne, M. J. Creech-Eakman, C. A. Haniff, C. A. Jurgenson and J. S. Young, "A high-sensitivity near-infrared science combiner for MROI," in *Optical and Infrared Interferometry*, M. Scholler, W. Danchi, and F. Delplancke, eds., Proc. SPIE **7013**, 701325-701325-11 (2008).
18. P. Coudray, J. Chisham, M. P. Andrews, I. Najafi, "Ultraviolet light imprinted sol-gel silica glass low-loss waveguides for use at 1.55 μm," Opt. Eng. **36**, 1234-1240 (1997).
19. P. J. Moreira, P. V. S. Marques, and A. P. Leite, "Hybrid sol-gel channel waveguide patterning using photoinitiatorfree materials," IEEE Photon. Technol. Lett. **17**, 399-401 (2005).
20. S. Olivier, L. Delage, F. Reynaud, V. Collomb, M. Trouillon, J. Grelin, I. Schanen, V. Minier, J. E. Broquin, C. Ruilier and B. Leone, "MAFL experiment: development of photonic devices for a space-based multiaperture fiber-linked interferometer," Appl. Opt. **46**, 834-844 (2007).
21. A. Ghasempour, A. M. P. Leite, F. Reynaud, P. V. S. Marques, P. J. V. Garcia, D. Alexandre, and P. J. Moreira "Hybrid sol-gel planar optics for astronomy," Opt. Express **17**, 1970-1975 (2009).
22. S. Vergnole, L. Delage and F. Reynaud, "Accurate measurements of differential chromatic dispersion and contrasts in an hectometric silica fibre interferometer in the frame of OHANA project," Opt. Commun. **232**, 31-43 (2004).

1. Introduction

Long baseline astronomical interferometry is a key technique to collect high angular resolution information of celestial objects. The complex visibility of the interferometric fringes is proportional to the Fourier transform of the object intensity distribution according to the Van-Cittert Zernike theorem [1]. Guided optics technologies proved to offer appealing capabilities in the context of astronomical instrumentation, and a few examples can be cited. Fiber Bragg gratings have been used to suppress OH-emission lines of the night sky spectrum [2], and large mode area photonic crystal fibers have been proposed for broadband light transportation, operating in the single-mode regime almost independently of the wavelength [3]. As astronomical signal beams are usually highly multimode, it has been proposed to adiabatically couple a multimode waveguide to a 3D array of single-mode waveguides for correct signal processing [4]. The stationary-wave integrated Fourier transform spectrometry (SWIFTS) concept will eventually lead to all-in-the-chip spectrometry, which would be ideal especially for space spectroscopic applications [5, 6]. So far, however, the main application of integrated optics (IO) in astronomical interferometry instrumentation has been for telescope beam combination.

The use of IO devices for beam combination was proposed in 1999 [7], and was followed

#122663 - $15.00 USD Received 12 Jan 2010; revised 28 Mar 2010; accepted 29 Mar 2010; published 21 Apr 2010

by several laboratory demonstrations [8, 9, 10]. The first astronomical validation of an integrated optics beam combiner was performed on the IOTA interferometer, where the H-band light (1.43-1.77 μm) of two telescopes was coherently combined [11]. The second on-the-sky example was a two beam combiner working in the astronomical K-band (2.0-2.4 μm), which was validated in the Very Large Telescope Interferometer (VLTI) [12]. Benisty et al. [13] characterized a new four beam combiner (to be used in VSI and in GRAVITY, both VLTI second generation instruments). The device is based on pairwise combination: for each pair of beams, four signal outputs in quadrature are produced (ABCD like), so the amplitude and the phase of the fringes are both retrieved using appropriate processing. For combination of six or more telescope beams, LeBouquin et al. [14] demonstrated that the most efficient design, in terms of signal-to-noise ratio, is a spatial all-in-one beam combiner (a configuration similar to a Young's interferometer). For combination of six telescope beams, VSI plans to use a multi-axial combiner [15]. The Swift-Gabor principle was suggested for combination of eight and more telescope beams [6].

In this rapidly evolving field of research, a fast prototyping technique would help to test new ideas and optimize designs. Such technique will be able to provide laboratory prototypes at low cost and with fast turnaround. Thus, after the design goals have been met, the results obtained employing this technology can be easily transferred to the production of a final field usable device fabricated using an adequate high performance technology (such as silica-on-silicon, in the case of integrated beam combiners or spectrometers). This is the case of the hybrid sol-gel technology, which has been associated with the UV laser direct-write technique or the conventional mask lithography to demonstrate integrated beam combiners. This paper presents the demonstration of this fast prototyping approach through the results obtained on the interferometric characterization of coaxial two, three and four beam combiners which were microfabricated using the hybrid sol-gel technology. In particular, for the first time, a coaxial integrated optics beam combiner, combining four telescopes, was fabricated and characterized. This beam combiner is the integrated optics analog of the bulk optics pupil-plane beam combiner used to obtain the first images from the four telescope optical interferometer COAST [16]. Similar bulk beam combiners are under study for the Magdalena Ridge Optical Interferometer [17]. The study of fringe visibility for the fabricated beam combiners is detailed and it is shown that the results of the spectral and temporal analyses are in mutual agreement.

2. Design, fabrication and interferometric testing

The hybrid sol-gel technology employed defines the fundamental parameters of waveguide fabrication, which are subsequently adopted in the computational design of the IO combiner chips. The devices produced were tested using an interferometric technique based on a Mach-Zehnder setup.

2.1. Hybrid sol-gel technology

The hybrid sol-gel technology used to produce IO devices is based on a low temperature process, which results in thick photo-patternable optical layers from a single deposition step, and avoids relatively complex and costly processing steps, such as ion etching [18]. The organic-inorganic material is synthesized from the precursor methacryloxypropyltrimethoxysilane (MAPTMS) by hydrolysis and polycondensation. Addition of zirconium (IV) propoxide mixed with methacrylic acid allows refractive index tuning of the MAPTMS-ZrO_2 material, as required to create the waveguide index profile. The solution is deposited on a glass substrate by spin-coating, and the films are pre-baked to evaporate the solvent. Channel waveguides and integrated optic devices have been fabricated in our group using MAPTMS-ZrO_2 and UV laser patterning by standard mask lithography or direct-write technique, without recourse to a photo-

#122663 - $15.00 USD Received 12 Jan 2010; revised 28 Mar 2010; accepted 29 Mar 2010; published 21 Apr 2010

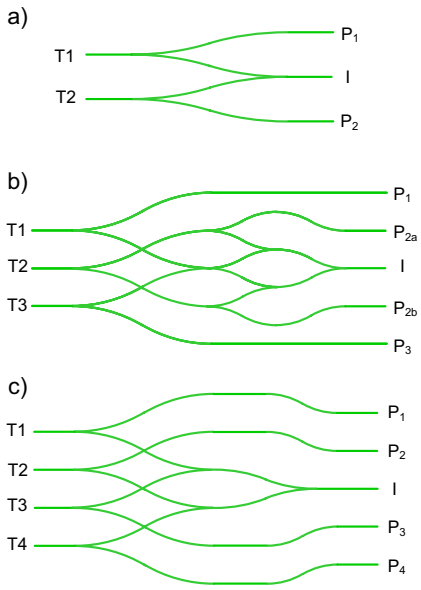

Fig. 1. Schematic layouts of 2T, 3T and 4T combiners.

initiator, and employing a standard photolitographic technique [19]. Refractive indices of core and cladding at the wavelength of 1.3 μm are, respectively, $n_{\text{core}} = 1.5096$ and $n_{\text{clad}} = 1.4998$. Single mode channel waveguides were fabricated with a square core cross section (typically 4×4 μm^2) and step index profile. The propagation loss measured in the single mode channel waveguides is typically 0.4 dB/cm at 1.3 μm, which is fully acceptable from the point-of-view of rapid prototyping.

2.2. Design

IO telescope beam combiners can be designed and operated in several ways [14]. The set of optical beams can be combined using pairwise, partial or all-in-one schemes (baseline coding). The light modulation of single mode beam combiners can be temporal, spatial or matricial (fringe coding). Hence, these different approaches result in 9 possible combination types. The advantages and drawbacks of each type of combination depend on the number of telescope beams to be combined. Here, only the temporal all-in-one combination is addressed employing a coaxial scheme (similar to a Michelson interferometer). Figure 1 shows the schematic layout of the coaxial two, three and four telescope beam combiners (hereafter denoted as 2T combiner, 3T combiner and 4T combiner) discussed below. The interference fringes resulting from the combination of all pairs of beams are simultaneously present in the single interferometric output channel. In each scheme, T_i is a telescope beam input, I is the interferometric output channel, and P_i designates a photometric output that provides information on T_i input power (to be used

#122663 - $15.00 USD Received 12 Jan 2010; revised 28 Mar 2010; accepted 29 Mar 2010; published 21 Apr 2010

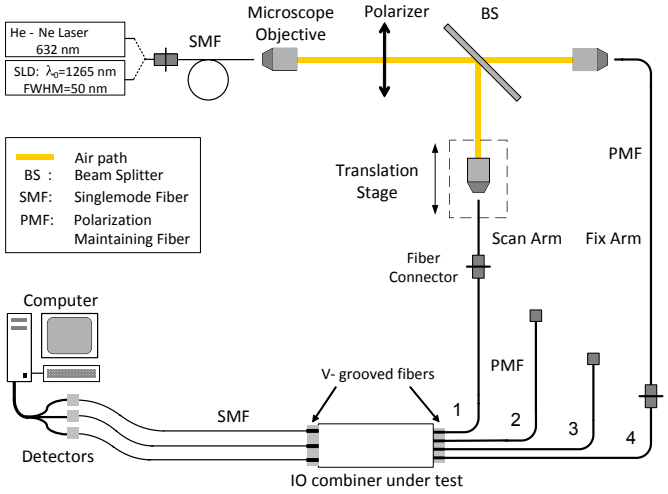

Fig. 2. Interferometric setup used for characterization of the beam combiners.

for correction of power unbalance, as discussed below). The design of a coaxial all-in-one beam combiner for an even number N of input beams follows almost directly from the design of the simple 2T combiner as follows from inspection of the examples of Fig. 1. However, in the case of an odd number N, the design is more complex, as it is of fundamental importance to ensure that all the interfering light paths have the same optical length in order to achieve correct broadband operation.

In an all-in-one combiner, all the inputs are combined coherently in the same output channel. For more than two beams, this will result in a complex interferogram pattern. Hence, in order to be able to separate the information regarding the interference of each pair of beams, the total interference pattern is processed in the Fourier domain. The input beams must be time modulated, using a set of modulation frequency values that leads to a non-redundant set of modulation frequencies in the interference of beam pairs [20] in order to avoid mixing of the information corresponding to the interference of each individual beam pair.

The design of the beam combiners was developed for operation in the astronomical J-band (1.1-1.4μm), using BPM-CAD commercial software packages (Optiwave and Rsoft). Specific aspects of design optimization dealt with Y-splitter/combiner and X-crossing sections, and overall optical path equalization in order to obtain high contrast broadband interferences.

2.3. Characterization setup

Figure 2 shows the experimental setup which was used for interferometric validation of the beam combiners. A He-Ne laser was used for preliminary alignments. A superluminescent diode (SLD), with emission centered at 1265 nm and with a spectral FWHM of 50 nm, was used as a broadband source for a full characterization of the combiners. The light source was coupled into a single mode fiber (SMF) which acts as spatial filter, then collimated and passed through a polarizer, and finally split into two beams, which were then injected into polarization maintaining (PM) fibers. In one arm of the Mach-Zehnder testing interferometer, a translation stage was used to balance the optical paths and to perform path scanning. Light was injected

#122663 - $15.00 USD Received 12 Jan 2010; revised 28 Mar 2010; accepted 29 Mar 2010; published 21 Apr 2010

into the IO beam combiner under test employing PM fibers inserted into a V-grooved holder. The outputs of the chip were coupled to standard single mode fibers, which fed single-pixel detectors. In the experiments described below, due to a setup design limitation, only two inputs of the combiner device could be fed at a time and hence, each pair of inputs was tested individually. In order to measure the visibility of the interferogram of the combination of each input pair, the raw interferogram was corrected from photometric unbalance of the inputs, using the signals from the photometric outputs of the chip. The resulting interferogram signal is referred as the normalized interferogram (I_n), whose values are in the range [-1,1], and whose visibility is then estimated by

$$V = \frac{\max(I_n) - \min(I_n)}{2} \tag{1}$$

A detailed description of the steps involved in data reduction can be found in [21].

3. Chromatic differential dispersion analysis

The visibility (V) of the normalized interferogram obtained from the IO device can be degraded by several mechanisms, among them chromatic differential dispersion inside the chip. In order to measure the chromatic differential dispersion, a spectral analysis of the interferometric output was performed, following an approach previously used to characterize an hectometric fiber interferometry system in the J-band [22]. The analysis described in this section, and its application to the results presented in the next section, specifically allowed the separation of the effects resulting from the test setup from those of the IO chip. Light from the interferometric output of the chip was coupled to an optical spectrum analyzer (OSA), and an example of the resulting channeled spectrum is shown in Fig. 3. The spectrum of the interferometric mixing of two inputs, as implemented via the setup of Fig. 2 (including air, fiber and IO chip paths), is given by [22]

$$B(\nu) = B_1(\nu) + B_2(\nu) + 2\sqrt{B_1(\nu)B_2(\nu)}C(\nu)\cos[\phi(\nu)] \tag{2}$$

where $\phi(\nu)$ is the spectral phase shift, $B_1(\nu)$ and $B_2(\nu)$ are the spectral power densities at each arm of the interferometer, and $C(\nu)$ is the contrast. The spectral phase shift, which is the frequency dependent phase difference between the two interfering beams, can be written as

$$\phi(\nu) = \phi_0(\nu) + \phi_f(\nu) + \phi_c(\nu) \tag{3}$$

where ϕ_0, ϕ_f and ϕ_c are, respectively, the spectral phase shifts in air, in the fibers and inside the chip. Throughout the next discussion, air is considered to be a non-dispersive medium. Hence the contribution of air paths to the spectral phase shift is

$$\phi_0(\nu) = k\Delta L = \frac{2\pi\nu}{c}\Delta L = \frac{2\pi\Delta L}{c}(\nu_0 + (\nu - \nu_0)) \tag{4}$$

where ΔL is the optical path difference in air and ν_0 is the mean frequency. For propagation in the two fibers and inside the chip, different propagation constants are attributed to each fiber (β_{f1}, β_{f2}) and to each path inside the chip (β_{c1}, β_{c2}). The contributions of fibers and chip waveguides to the spectral phase shift, after Taylor expansions of the propagation constants around the mean frequency (ν_0), are

$$\phi_f(\nu) = \beta_{f1}(\nu)L_{f1} - \beta_{f2}(\nu)L_{f2} = \sum_{i=0}^{n}\left(\frac{\partial^i\beta_{f1}}{\partial\nu^i}L_{f1} - \frac{\partial^i\beta_{f2}}{\partial\nu^i}L_{f2}\right)\frac{(\nu-\nu_0)^i}{i!} \tag{5}$$

$$\phi_c(\nu) = \beta_{c1}(\nu)L_{c1} - \beta_{c2}(\nu)L_{c2} = \sum_{i=0}^{n}\left(\frac{\partial^i\beta_{c1}}{\partial\nu^i}L_{c1} - \frac{\partial^i\beta_{c2}}{\partial\nu^i}L_{c2}\right)\frac{(\nu-\nu_0)^i}{i!} \tag{6}$$

#122663 - $15.00 USD Received 12 Jan 2010; revised 28 Mar 2010; accepted 29 Mar 2010; published 21 Apr 2010

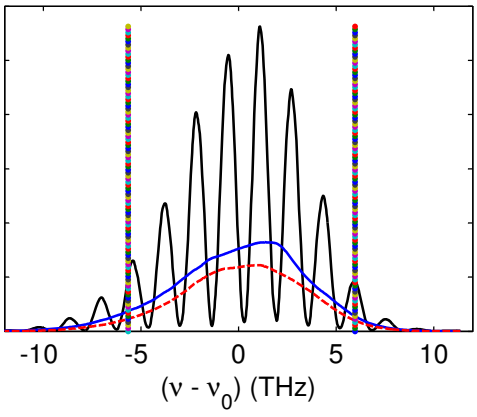

Fig. 3. Channeled spectrum $B(\nu)$ and spectral power densities $B_1(\nu)$ and $B_2(\nu)$. The two vertical lines show the selected window used for calculation of the chromatic differential dispersion.

Hence, the spectral phase shift can be written, in general form, as a polynomial function of frequency:

$$\phi(\nu) = a_0 + a_1(\nu - \nu_0) + a_2(\nu - \nu_0)^2 + a_3(\nu - \nu_0)^3 + ... \tag{7}$$

Looking at the description of ϕ_0 from Eq. (4), it is clear that it only contributes to coefficients a_0 and a_1. So when there is no global differential dispersion in the setup, the first order polynomial completely describes the spectral phase. When there is chromatic differential dispersion, higher orders appear in $\phi(\nu)$ formula: a_2 and a_3 are coefficients of second- and third-order differential dispersion, which arise from the characteristics of the input fibers and/or of the light paths inside the chip.

The chromatic differential dispersion can be evaluated by substituting the measurements of $B(\nu)$, $B_1(\nu)$ and $B_2(\nu)$ (see Fig. 3) in Eq. (2) to calculate $\cos[\phi(\nu)]$ from the experimental data. Using $\phi(\nu)$ from Eq. (7) into $\cos[\phi(\nu)]$, the parameters a_2 and a_3 can be extracted by fitting. In order to cross-check the obtained values of a_2 and a_3, they can be substituted in Eq.(8) to compute a simulated visibility function of the interferogram, given by

$$V_{simul}(x) = \left| \frac{\int B(\nu)\, e^{j\phi(\nu,x)} d\nu}{\int B(\nu)\, d\nu} \right| \tag{8}$$

where x is the optical path difference.

4. Results and discussion

For characterization of the beam combiners, both temporal and spectral analyses have been performed. The results are listed in Table 1, where the V values are visibilities obtained from the analysis of the fringe patterns resulting from temporal scanning (see Fig. 4). As mentioned before, only two inputs could be simultaneously launched into the chip. Hence, for the 3T combiner and 4T combiner devices, the visibilities were measured for all possible input pairs. In Table I, the first column indicates the beam combiner and the second column the analysed combination pair. In the top part of Fig.4, an interferogram from a 2T combiner (with $V = 98.7$) is shown. In the middle and bottom parts of the same figure, interferograms with respectively the best and the worst visibility values from the 4T combiner (combination pairs, 24 with $V = 97.5$,

#122663 - $15.00 USD Received 12 Jan 2010; revised 28 Mar 2010; accepted 29 Mar 2010; published 21 Apr 2010

Table 1. Visibilities of all combination pairs of the 2T, 3T and 4T combiners. V is the experimental visibility of the normalized interferogram. The values of a_2 and a_3 were measured using spectral analysis. V_{simul} is the visibility of the interferogram which was calculated using the experimental a_2 and a_3 values. The uncertainties quoted in columns 4 and 5 are valid for a confidence level of 0.7 ($\pm\sigma$). Uncertainties of the V and V_{simul} values are respectively smaller than 0.3 and 0.2 percent.

Beam combiner	Combination pair	V (%)	a_2 (mrad THz^{-2})	a_3 (mrad THz^{-3})	V_{simul} (%)
2T	12	98.7	2.16 ± 0.35	0.34 ± 0.10	99.7
3T	12	98.1	0.69 ± 0.07	1.11 ± 0.04	98.7
3T	23	95.8	2.64 ± 0.10	1.87 ± 0.04	96.8
3T	13	95.1	4.72 ± 0.06	0.02 ± 0.03	99.4
4T	12	93.4	13.44 ± 0.47	2.49 ± 0.13	93.2
4T	23	96.3	11.64 ± 0.37	1.20 ± 0.11	95.7
4T	34	96.8	10.49 ± 0.27	0.36 ± 0.18	97.1
4T	13	96.9	12.76 ± 0.22	1.40 ± 0.07	95.0
4T	24	97.5	3.57 ± 0.28	1.15 ± 0.05	98.2
4T	14	92.1	15.31 ± 0.36	1.07 ± 0.11	94.1

and 14 with $V = 92.1$) are shown. Interferograms obtained from the 3T combiner can be found in [21].

The comparison of the V values from 4T and 3T combiners with the value from the 2T combiner shows some degradation. In general terms, there are several mechanisms which can cause the observed visibility decay: spatial mode mismatch, polarization mismatch, or chromatic differential dispersion between the two interfering fields. As only single mode waveguides are used in this work, spatial superposition of the interfering lights is achieved perfectly, so this factor can be dropped. The results of the spectral analyses help to discriminate whether polarization or dispersion problems are responsible for the visibility decay. In Table 1, a_2 and a_3 are coefficients of second- and third-order differential dispersion, which were measured using spectral analysis of the channeled spectra. Each value of these coefficients is the average of 5 to 10 measurements. V_{simul} is the maximum visibility of the interferogram, which was calculated using Eq. (8) and the measured a_2 and a_3 values. Comparing V with V_{simul} values of 3T and 4T combiners, very good agreement between them can be verified (small differences can be attributed to polarization mismatch in the fiber connectors). This good agreement shows that dispersion is mainly responsible for the visibility decay.

After showing that the chromatic differential dispersion is the cause of visibility degradation in the 3T and 4T combiners, the next step is to identify its origin: the input fibers or the light paths inside chip. In order to distinguish the contributions of the fibers from those of the chip, a reference 2T combiner was used for characterization of the setup. With this combiner inserted in the setup, visibility measurements were carried out with different combinations of fiber inputs (because of the fixed separation of the inputs of the 2T combiner, only interferometer light paths leading to the V-groove which were next to each other, i.e. 12, 23 and 34 could be used by the 2T combiner). The results of this characterization showed that the setup always gives a visibility higher than 98.4, and a_2 and a_3 values always lower than 2.33 (mrad THz^{-2}) and 0.34 (mrad THz^{-3}). If 3T or 4T combiner devices, combine exactly the same interferometer light paths, which were characterized using the reference 2T combiner, it can be discriminated whether their associated visibility decay, as compared to the value from the reference 2T combiner, has its origin inside the chip or from the external measurement setup. For example, in the 4T

#122663 - $15.00 USD Received 12 Jan 2010; revised 28 Mar 2010; accepted 29 Mar 2010; published 21 Apr 2010

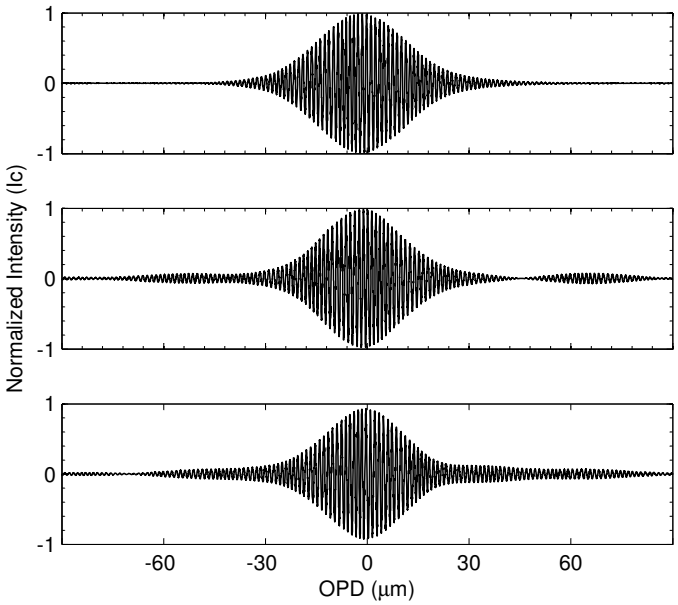

Fig. 4. Normalized interferograms as measured for different combiners. Top: Interferogram of the 2T combiner with $V = 98.7$. Middle and bottom: Interferograms of the 4T combiner with best and worst visibilities, for combination pairs 24 with $V = 97.5$, and 14 with $V = 92.1$.

combiner, combination pairs of 12, 23 and 34 are the same interferometric paths as those which were characterized by the reference 2T combiner, and they display smaller V values, and higher a_2 and a_3 values, than the values obtained with the reference 2T combiner; hence, by comparing them, it can be concluded that the visibility decay is originating inside the chip.

The next step would be to find which features inside the chip create the chromatic differential dispersion which causes the visibility degradation of 3T and 4T combiners. Equation (5) reveals that the dispersion inside the chip can arise from geometrical path differences inside the chip or/and from propagation constant differences inside the chip. The geometrical paths inside the chip were designed to be equal, although cleavage errors can introduce some deviations that should be small in any case. So, we can claim that the main reason for differential dispersion inside the chip is the difference in waveguide modal propagation constants, which is caused by the residual inhomogeneity of the film layer used to fabricate the channel waveguides.

The conclusions extracted are specific to the demonstrator devices fabricated by the hybrid sol-gel fast prototyping technique. This fabrication technology results in step-index rectangular/square section waveguides, as does the silica-on-silicon technology which offers lower propagation loss and is typically used to fabricate high performance passive integrated components for field applications. Therefore, similar design layouts are shared between the two technologies, and the characterization approach described here are also applicable to the field usable devices, with obviously different results.

5. Conclusion

The hybrid sol-gel technology has been used for fabrication of prototypes of coaxial two, three and four telescopes beam combiners for astronomical applications. In particular, for the first time, a coaxial integrated optics beam combiner, combining four telescopes, was fabricated

#122663 - $15.00 USD Received 12 Jan 2010; revised 28 Mar 2010; accepted 29 Mar 2010; published 21 Apr 2010

and characterized. An interferometric setup was used which allowed both temporal and spectral analyses of the beam combiners. The characterization method results were cross checked with the contrast measurements, demonstrating that chromatic differential dispersion is the main contributer to the observed contrast reduction. However, high contrast fringes were measured using temporal analysis, thus confirming that the procedures used lead to performant IO beam combiners. The results demonstrate the capabilities of the hybrid sol-gel technology for fast prototyping of complex chip designs for astronomical applications.

Acknowledgements

This work was partially supported by grant PTDC-CTM- 72093-2006, and AG, DA and PJVG acknowledge the grants SFRH/BD/24493/2005, SFRH/BD/39284/2007 and SFRH/BSAB/806/2008, respectively, all awarded by FCT and POCI, with funds from the European Union programme FEDER.

#122663 - $15.00 USD Received 12 Jan 2010; revised 28 Mar 2010; accepted 29 Mar 2010; published 21 Apr 2010